OXIDATION BEHAVIOUR OF FE-CR-NI ALLOYS IN SUPERCRITICAL WATER

MANUELA FULGER, MARIA MIHALACHE, LUCIAN VELCIU, DANIEL PETRESCU

Institute for Nuclear Research (RATEN ICN) Pitesti, Romania
e-mail: manuela.fulger@nuclear.ro

Abstract

Supercritical water cooled reactors (SCWR) are promising generation IV nuclear reactors which provide a much higher thermal efficiency and are simpler to construct than current light water reactors. Selecting proper candidate materials is one of the key issues for the development of the supercritical water-cooled nuclear reactors because the corrosion becomes a challenging problem. Austenitic Fe-Cr-Ni alloys are generally considered as materials having good corrosion resistance. Among the major constituent elements of materials, Cr can promote development of a protective layer oxide, while Ni can enhance the stability of the oxide layer. The morphologies, microstructures and chemical composition of the oxides films may give significant clues to understanding the corrosion process and finding ways to prevent corrosion in supercritical water. To rationalize the corrosion resistance of candidate austenitic Fe-Cr-Ni alloys in supercritical water, this work was focused on investigating the oxidation behaviour of some alloys: high chromium containing alloys (310H and Incoloy 800HT) and medium chromium containing alloys (304L and 316L). After exposure in water at 550^{o}C and 600^{o}C, with 25MPa pressure for up to 1680 hours, the studied materials were characterized by recording oxide growth and oxidation kinetics using mass change, recording the oxide morphology by optical microscopy and scanning electron microscopy (SEM/EDS), and comparing all of the stated oxidation behaviour. The weight change decreased with increased Cr content, at both temperatures, for all investigated alloys. After testing, it was determined that internal oxidation or secondary phases (sigma phase) may occur in some alloys exposed in supercritical water

Keywords: *Fe-Cr-Ni alloy, Supercritical water, Internal oxidation*

Introduction

Based on the working conditions, the SCWR operating temperature and pressure are designed to exceed the thermodynamic critical point of water. Water above a temperature of 374.15 °C and a pressure of 22.1 MPa there is in supercritical state and acts as a dense gas, exhibiting properties significantly different from that of water below the critical point.

The corrosion performance of candidate materials in supercritical water (SCW) environment can be affected by several factors, such as temperature, pressure, material composition, material structure, water chemistry, and exposure time. Oxidation, which is the most encountered form of high-temperature water corrosion, is not always detrimental, since most heat resistant alloys rely on external oxidation in the form of a protective oxide film which provides resistance to this type of corrosion.

A good selection of the high-temperature alloys can minimise excessive metal loss by scale formation (external oxidation) and penetration of oxidation products into the alloy (internal oxidation). To exhibit good protective properties in high-temperature water, the oxide layers developed on the alloys must have sufficient thickness and should be very stable, adherent and continuous [1].

For selection of best alloys to use in supercritical water it will be necessary to include some materials as benchmark for which there is substantial information about behaviour in various nuclear reactors (PWR/BWR, CANDU). These benchmark materials provide a basis to identify an acceleration of known phenomena, or the development of new phenomena in supercritical conditions.

The austenitic stainless steels contains sufficient Cr in their composition to allow development of a protective chromium rich oxide layer in the form of Cr_2O_3 during oxidation at high temperatures developed in SCW [2]. Therefore, selecting an alloy which will maintain the integrity of the passivation layer at the supercritical conditions is a crucial requirement in choosing a material for fuel cladding and other components SCWRs.

The 304-type austenitic stainless steel is used in conventional power plants where environment temperatures are below 600 ^{o}C [3]. To eliminate the harmful effect of carbon on its corrosion resistance was developed 304L-type, steel with low carbon content [4]. AISI 310H-type is a 300-series chromium-nickel austenitic stainless steel that starts on 304-type stainless steel, with chromium and nickel additions for strength and oxidation resistance.

The 800HT alloy was also selected as candidate in the SCWR design due to its advantages in high strength and corrosion resistance at elevated temperatures and corrosive atmospheres [5]. The chemical composition of 800HT alloy is placed on the border of stainless steels and Ni base alloys even if it is designated as a Ni base alloy. However, 800HT alloy has a restricted chemistry, within the limits of 800H-type alloy, and requires a heat treatment of 1149°C as a minimum temperature.

In the case of 800HT alloy, the contents of aluminium and titanium are maintained in upper limit of the specified material range, so they are expected to have higher creep and stress rupture properties than 800H alloy [6, 7].

In this study, the corrosion performances of two austenitic stainless steels (304L, 310H) and one Ni base alloys (800HT) have been investigated in supercritical water at temperature range of 550-600°C under a pressure of 25MPa. Oxide morphology and samples microstructures were revealed using SEM microscopy / EDX analysis or optical microscopy while oxidation kinetics was recorded using specific mass gain over time.

Experimental

In this study, commercial AISI 304L, AISI 316L and AISI 310H steels, as well as Incoloy 800HT have been used. The nominal chemical compositions of the materials (in weight percent) are listed in Table 1.

As it is shown, the selected alloys chemical composition differs mainly by content of chromium and nickel. Because there is an extensive data base for stainless steels at low temperatures, specimens of 304 stainless steels, including L variants, are considered as benchmark materials. The tested materials were as cold rolled sheets; 310H steel was as heat treated at 1100 °C followed by water quenching, while 800HT was pickled, washed and dried.

Table 1. Chemical composition of tested alloys [wt %]

Alloy	C	Mn	Si	Cr	Ni	Mo	P	S	Fe	N	Ti	Al
316L	0.019	1.55	0.45	***16.71***	***11.33***	2.11	0.022	0.006	67.7	0.1	-	-
304L	0.030	1.37	0.46	***18.07***	***8.11***	-	0.028	0.0006	71.9	-	-	-
310H	0.063	1.61	0.71	***24.13***	***19.03***	-	0.016	0.001	54.34	-	-	-
800HT	0.077	0.71	0.34	***20.06***	***31.22***	-	-	<0.001	45.19	-	0.52	0.51

Rectangular test coupons (25 × 15 × 2 mm) were cut from as received materials using a diamond wheel saw. A 2 mm diameter hole was then drilled out near the top of each coupon to facilitate mounting the coupons on a coupon tree during the experiment. Prior to being exposed in autoclaves, the as received coupons were polished with abrasive papers up to 1200 grade, followed by ultrasound cleaning in acetone and drying.

A static autoclave test facility made of Alloy 625 with a total chamber volume of 945 ml was used for the exposure of the coupons. Oxidation tests have been performed in deionized water at 550 – 600 °C and the pressure was kept constant at 25 MPa, to maintain supercritical conditions.

The pH of deionized water was about 6.7, measured at room temperature, the conductivity being of ~ 0.2 μS/cm. The dissolved oxygen content during tests was maintained at about 2 ppm (oxygen releasing at 110 °C, based on Vukalovich calculations) [8]. Each coupon was weighed before and after exposure using an analytical balance with an accuracy of ±0.01 mg in order to determine the amount of weight gained (or lost) during the exposure.

The oxidation behaviour of the samples was analysed by means of scanning electron microscopy / energy dispersive X-ray spectroscopy (SEM/EDS) with TESCAN VEGA II-LMU equipment. To display the grain and interphase boundaries present in the representative area of each sample an optical microscope (OLYMPUS GX 71 type) was used. To reveal the grain boundaries/ outline carbides, the alloys were etched using 10% oxalic acid solution; in order to show the attack sigma phase the alloys were electrochemically etched in 10% KOH (or 10% NaOH) solution, for 60 s at 1.5-3V voltage.

Results and discussions

Weight change

The corrosion test specimens' weight was measured before and after the general corrosion test. After the test, the specimen surfaces were covered with oxide films. The obtained weight change consisted of gross information, including weight gain due to oxidation on the surface.

Fig. 1 shows the weight gain of the materials exposed for 1680 hours in supercritical water at 550 and 600 °C. All samples showed increased weight with temperature, so the oxidation rate is temperature dependent.

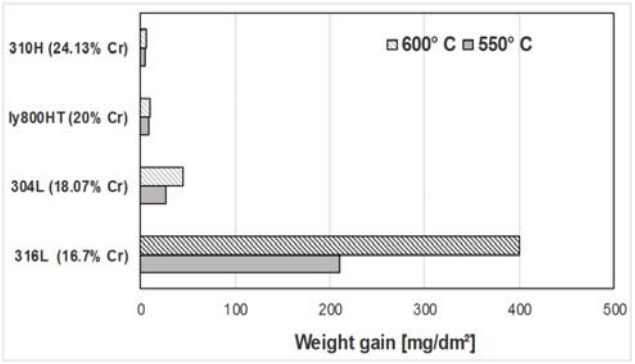


Fig. 1. Weight gain values as function of exposure time in supercritical water for: 316L, 304L, 310H and 800HT alloys

For the 310H alloy the weight gain was extremely small at both temperatures comparatively with all tested samples. Also, the weight gain in supercritical water decreased with increasing Cr content in alloys, in the following order: SS 316L > SS 304L > 800HT alloy > 310H steel.

By the contrary, the 316L alloy samples have presented the largest variations in weight, as function of temperature. Oxidation of the 316L and 304L samples was more seriously at both temperatures, comparatively with the other alloys. This is in agreement with the formation of porous oxide layers detected further by SEM onto the surfaces of these samples. 800HT alloy had comparatively mass gains at both temperatures.

To produce reliable oxidation kinetics for the samples tested at 550 ^{o}C and 600 ^{o}C, more data should be needed. General corrosion property could not be adequately evaluated with weight change before and after the general corrosion test because sometime oxide film spallation can cause underestimation of the general corrosion property.

Oxide layers thickness

After oxidation, the measuring of oxide scale thickness was performed. One coupon from each alloy was cold mounted in cross-section using epoxy resin for this purpose. The surface was prepared using standard metallographic procedures to create a mirror finish. After that, the thickness of coupons was measured using the optical microscope.

In Fig. 2, the optical micrographs are presented, showing the oxide layers formed on all alloys with the measured average thickness of the oxide layers.

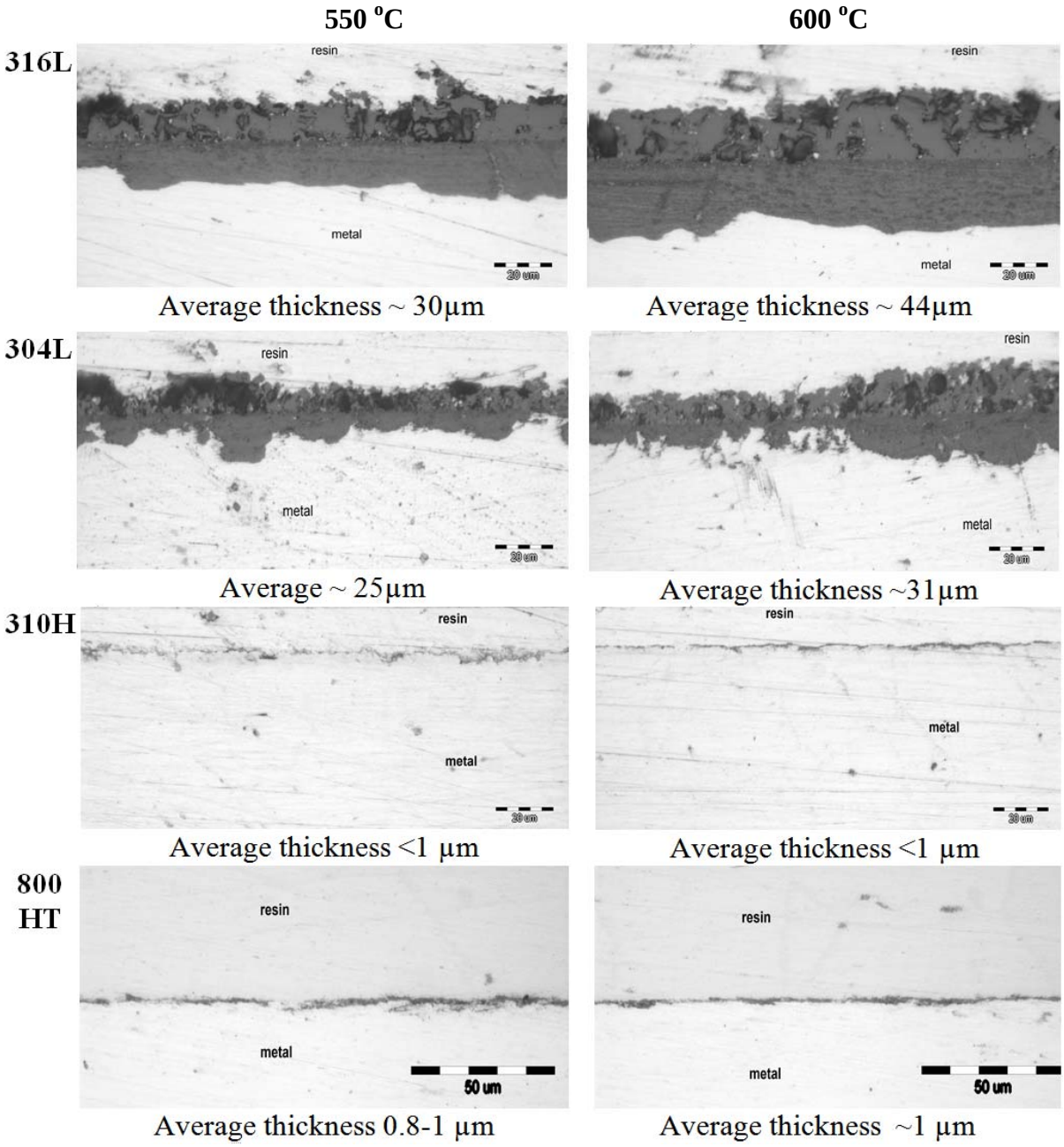


Fig. 2. Optical micrographs showing the formed oxide layers (x500 magnification) at: 550 ^{o}C (left) and 600 ^{o}C (right)

The data obtained by optical microscopy are consistent with those obtained by weight gain analysis, where is evident the growing tendency of oxide layers with temperature, mainly in the case of 316L and 304L coupons. Additionally, it can be seen some ″mushroom″ shapes under the oxide layer which was assumed to be the result of the internal oxidation process.

Oxides scale characterization

The effect of the exposure temperatures (550^{o}C and 600^{o}C) and pressure on the morphologies of coupons surface is shown in Fig. 3, where significant differences can be observed between oxides developed during tests.

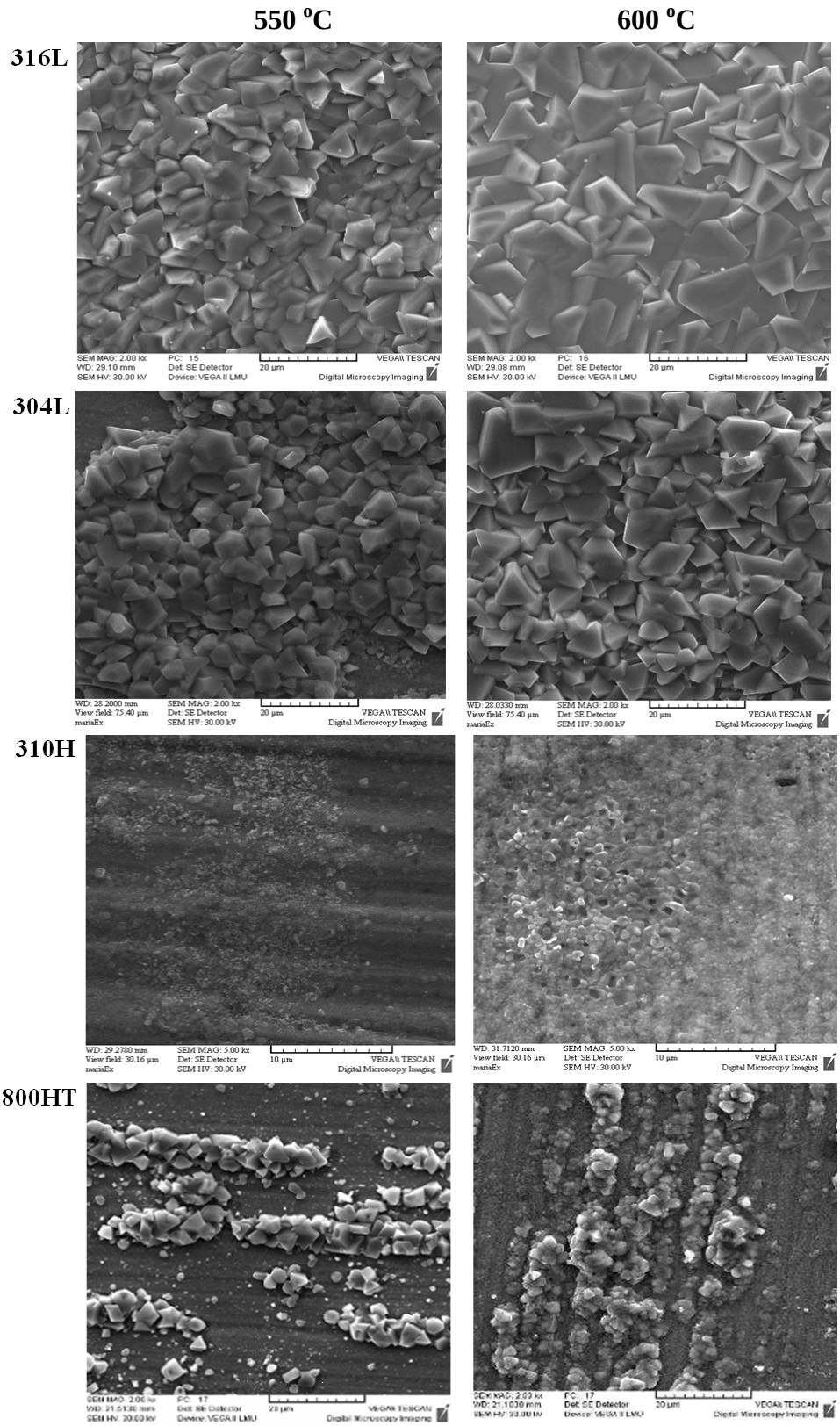


Fig. 3. SEM images of surface morphology for oxide films formed on tested alloys in supercritical water at: 550 ^{o}C (left) and 600 ^{o}C (right)

On the 316L and 304L alloys surface, a duplex oxide layer was developed at both temperatures. Generally, the oxide layer formed on the alloy 316L stainless steel exposed to the SCW is composed of two distinct layers: (1) iron rich oxides magnetite/hematite as the outer oxide layer and (2) Cr-rich spinel oxide as the inner oxide layer [9]. Inner and outer layers exhibit quite different characteristics in terms of composition and crystalline structure.

Generally, diffusion phenomena play a vital role in the formation of an oxide layer. The critical chromium concentration to transform less protective internal oxide ($FeCr_2O_4$) into more protective external oxide (e.g. Cr_2O_3) which blocks the O inward diffusion in austenitic Fe-Cr-Ni alloys is reported to be approximately 20 wt% [10].

However, the 316L alloy has about 16 wt% Cr content. Thus, although Cr_2O_3 forms in the initial stages of oxidation, it converts into $FeCr_2O_4$. It has been proposed that a spinel $FeCr_2O_4$ layer is less protective than a Cr-rich $[Mn, Cr]_2O_3$ layer since Fe diffusion in a spinel FeCr2O4 layer is three times faster than Cr, whereas Fe and Cr diffusion coefficients in a Cr_2O_3 layer are similar.

In the case of the 304L alloy, at 550 ^oC it can be observed the inner layer over which the magnetite and hematite crystals were developed. Among all samples exposed in SCW at 550 ^oC and 600 ^oC, the density of the oxide crystals was much higher on 316L samples.

After exposure in SCW, the 310H alloy samples showed interference colours, indicating a thin oxide scale formed onto the entire surface. It was very difficult to assess if on these samples two oxide layers were formed or not. In this case it was necessary a higher magnification (5000 or more) to observe the submicron oxide particles dispersed onto the samples surface. For both temperatures, on the surfaces of 310H samples very small crystallites were formed, as shown in Fig.3.

The 800HT alloy exposed at 550 ^oC showed strings of polyhedral crystallites developed over a uniform internal oxide layer. At 600 ^oC, the strings have thickened themselves and the crystallites shape becomes rounded. This duplex oxide layer structure is normal for Ni-base alloys. Generally, the outer oxide layer is rich in Ni and contains large crystals, while the inner oxide layer has fine crystals and is rich in Ni, Fe, Cr and Cr spinels [10].

Oxides structure

Fig. 4 shows the EDS compositional profile on a cross-section through one black cavity assumed to be internal oxidation zones oxide layer grown on 304L sample after 1680 h at 600 ^oC.

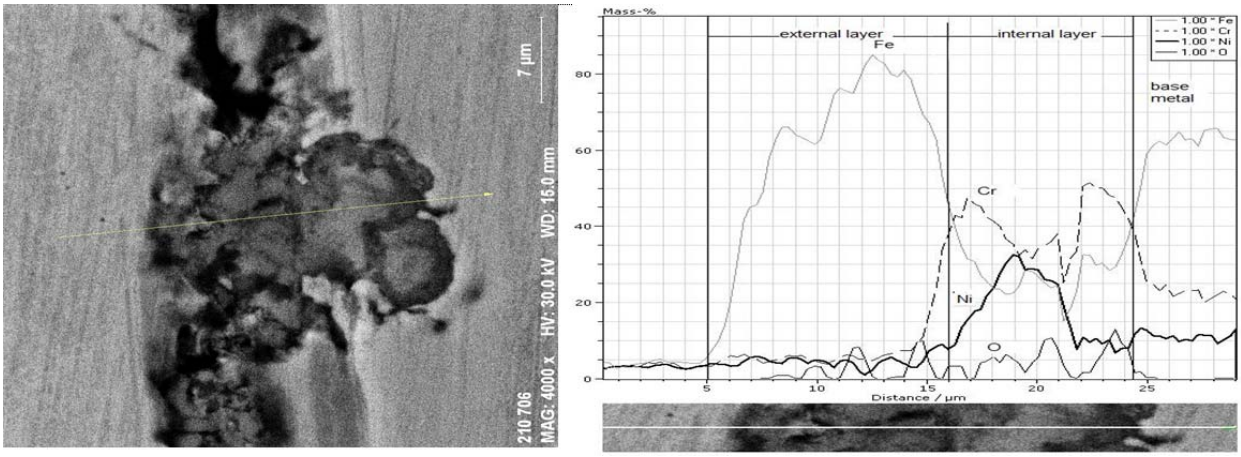


Fig. 4. Internal oxidation of 304L alloy exposed at 600^{o}C /250atm, revealed by SEM/EDS

The elemental depth profile displays an outer oxide film enriched in Fe and deficient in both Cr and Ni, while the inner layer contains high concentrations of Cr and Ni. On the bottom of the cavity, a higher concentration of chromium, iron and oxygen can be observed, indicating formation of a spinel oxide $FeCr_2O_4$ type. This was possible because the Cr concentration in 304L and 316L steels are about 18wt% and 16.71 wt% Cr, respectively. Long term exposure can lead to oxide film overlap, and oxidation may penetrate along Cr depleted grain boundary.

One possible explanation for internal oxidation process is the porosity of external oxide layer which allowed the diffusion of a greater amount of oxygen ions through the scale. Regardless of the explanation, it is certain that the internal oxidation of the 304L and 316L alloy along grain boundaries would be detrimental to mechanical properties such as ductility.

Microstructural analysis after oxidation

Fig. 5 shows SEM images revealing the grain boundary structures for 310H and 304L alloys oxidized at 550 ^oC and 600 ^oC for up to1680 h. In the case of 304L samples, after exposure in supercritical water at 600 ^oC, under oxide layer can be seen black cavities developed as result of internal oxidation.

On the bottom of the cavities are present spinels identified by EDS as being $FeCr_2O_4$. Also, as can be seen in Fig. 6, after exposure in water at 600 ^oC, the 304L alloy presents coarse grain boundaries with intergranular and intragranular carbides precipitates that suggest a susceptibility to intergranular attack as a result of the chromium depleted zones near the grain boundaries [11].

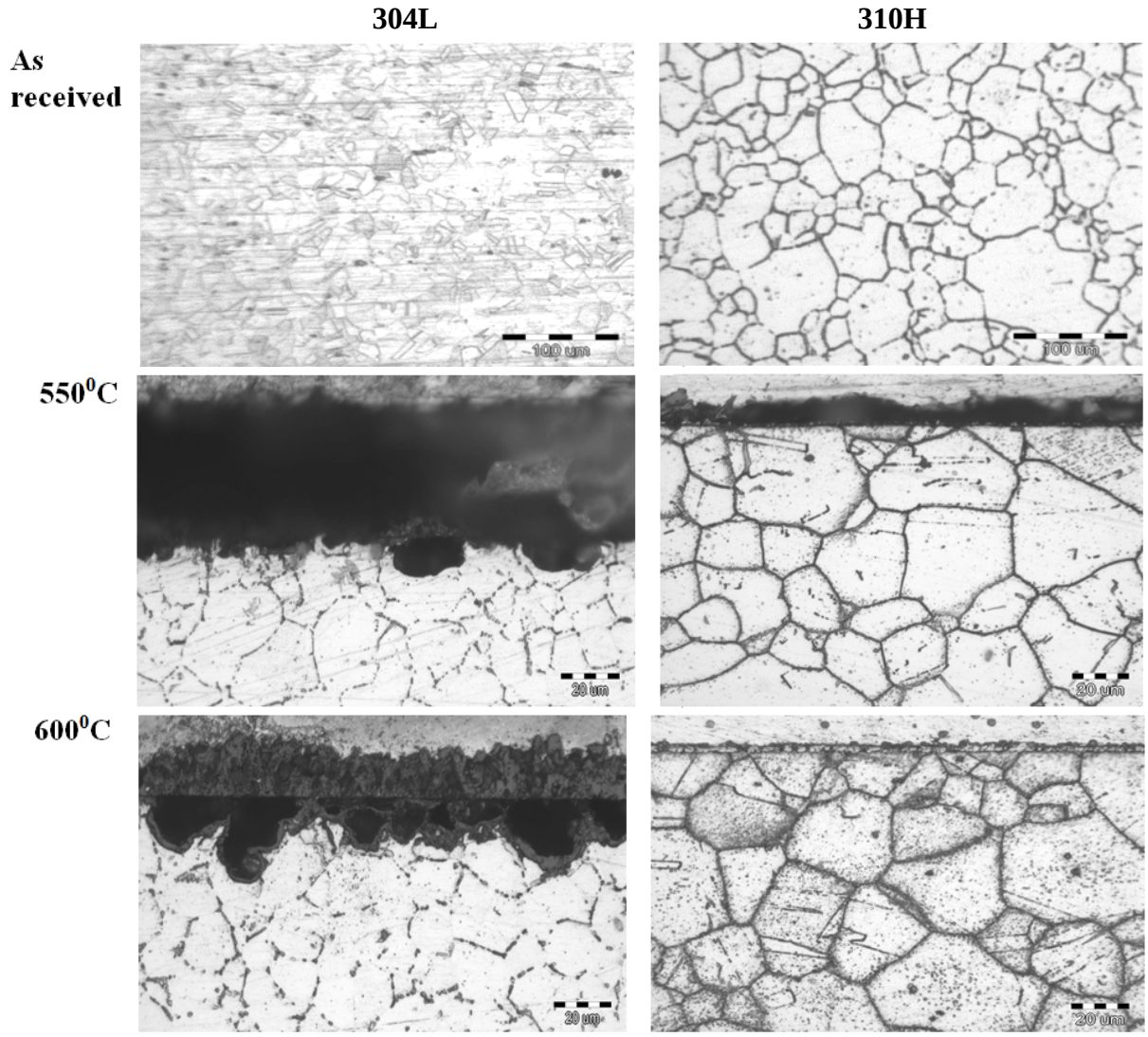


Fig. 5. SEM images showing grain boundaries structure of 304L (left) and 310H (right) alloys after testing in SCW

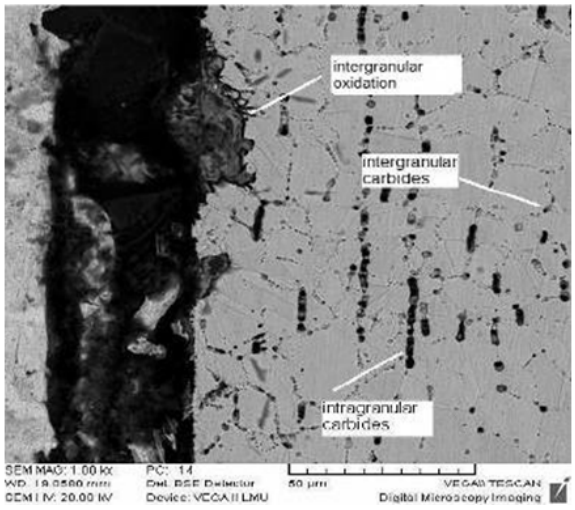


Fig. 6. SEM images of 304L microstructure after oxidation in water at 600^{0}C /250atm

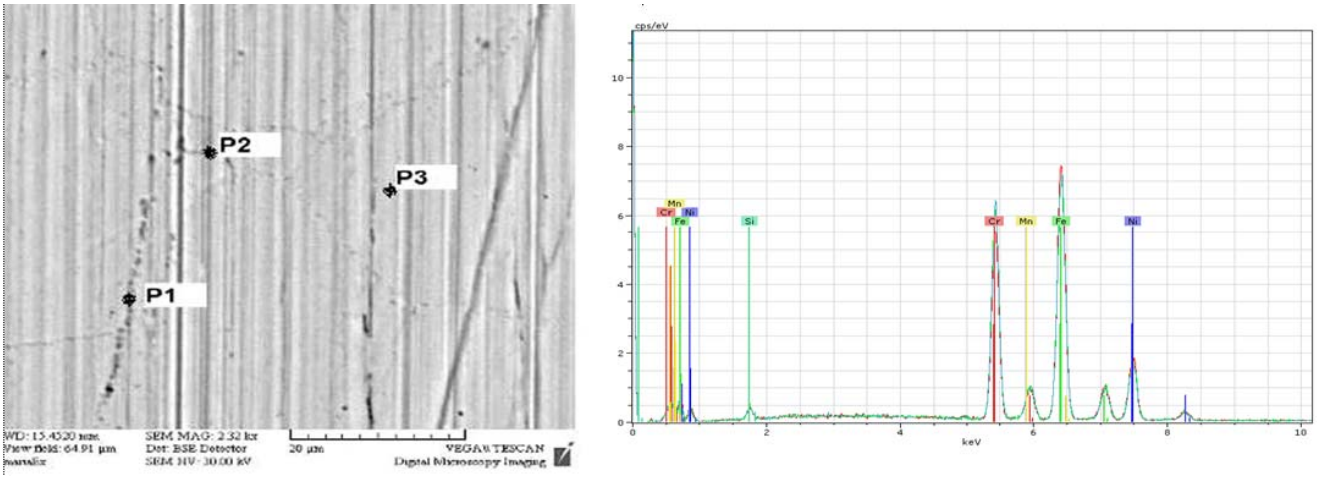
Even the 310H samples exhibited a thinner oxide layer after oxidation, the microstructural analysis points out coarse grain boundaries and larger grains at both supercritical temperatures.

In the same time, the microstructural analysis of 310H alloy points out the presence of detrimental sigma phase possibly due to the higher chromium content than the other alloys, which encourages sigma phase formation.

After electrolytic etching in 10% NaOH solution, the EDS analysis on spots has been performed on 310H sample in zones where the presence of sigma phase was suspected.

Fig. 7 shows higher concentrations of Cr in the spots P1 and P2 than in the base material at grain boundaries. The precipitation of the sigma phase is often observed in various series of stainless steels, being one of the main reasons for the deterioration of stainless steel properties (mechanical, corrosion resistance, and welldability).

The sigma phase can be precipitated under elevated temperature and this is difficult to be prevented when the Cr content is above 20 wt% in stainless steels [12].



Element [wt%]	Si	*Cr*	Mn	Fe
P 1	1.90	***28.39***	1.8	51.60
P 2	1.68	***27.15***	2.07	50.49
P 3	1.49	***24.34***	1.86	52.54

Fig. 7. SEM images of 304L microstructure after oxidation in water at 600^0C /250atm

Conclusions

A comparison of the austenitic Fe-Cr-Ni alloys behaviour in supercritical water shows that the oxidation is the main form of high-temperature corrosion.

In terms of mass gain, the 310S alloy had the best oxidation behaviour (the smallest weight gain respectively the thinner oxide layer), while the 316L alloy had the greatest weight gain respectively the thicker oxide layer.

The weight gain in supercritical water decreased with Cr content, in order: 316L > 304L > 800HT > 310H.

A number of phases can form within austenitic steels in water at high temperatures and pressures. The 310 S had the thinner oxide layer among all alloys, but is possible to develop detrimental sigma phase due to higher chromium content comparatively with the other alloys.

Even though the 304L steel has low carbon content, chromium carbides were identified in intergranular and intragranular sites after exposure in SCW. The precipitation of chromium carbide and sigma phase lead to sensitization of the steel, i.e., increases the susceptibility to intergranular corrosion.

The 800HT alloy did not form any precipitate phase during its oxidation in SCW. This may be explained by the relatively high nickel content (31.2%) which results in a more thermodynamically stable alloy that is more resistant to second phase precipitation.

In the case of 304L and 316L alloys, additionally occurred internal oxidation usually identified in alloys with Cr content lower than 20 wt%.

References

[1] Ostwald, C., Grabke, H.J. (2004) ″Initial oxidation and chromium diffusion. I. Effects of surface working on 9–20% Cr steels″, Corrosion Science, Vol. 46(5), pp. 1113-1127.

[2] Tan, L., Shridharan, K., Allen, T.R. (2006) ″ The effect of grain boundary engineering on the oxidation behavior of INCOLOY alloy 800H in supercritical water″, J. Nuclear Mater., Vol. 348(3), pp. 263-271

[3] Fulger, M., Radulescu, M., Lucan, D., Velciu, L., Manea, A.C. (2004) ″The corrosion kinetics of 304L stainless steel, of Incoloy 800 and of SA516 carbon steel in the secondary circuit of nuclear steam generator″, Rev. Chim. (Bucharest), Vol. 55(3), pp. 163-168.

[4] International Atomic Energy Agency (1999) ″Assessment and management of ageing of major nuclear power plants components important to safety: PWR vessel internals″, IAEA TECDOC no. 1119, pp. 14-18

[5] * * * (2004) ″Next Generation Nuclear Power Plant Materials Research and development Program Plan″, INEEL/EXT-04-02347, Idaho National Engineering and Environmental Laboratory, Bechtel Idaho
[6] * * * (2004) ″INCOLOY alloy 800H & 800HT″, Techn. Bull., Special Metals Publication SMC-047, available on http://www.specialmetals.com.
[7] Mankins, W.L., Lamb, S. (2002) ″Chapter: Nickel and nickel alloys″, in *Properties and Selection: Nonferous Alloys and Special Purpose Materials*, Vol. 2, Metals Handbook, ASM International
[8] Vukalovich, M., Rivkin, S.L., Aleksandrov, A.A., (1969) ″Tablitsy teplofizicheskikh svoistv vody i vodianogo para″, Moscow, Russia (in Russian).
[9] Behnamian, Y. Mostafaei, A., Kohandehghan, A. Amirkhiz, B.S., Serate, D., Sun, Y. et al. (2016) ″A comparative study of oxide scales grown on stainless steel and nickel-based superalloys in ultra-high temperature supercritical water at 800 °C″, Corrosion Science, Vol. 106, pp. 188–207.
[10] Fulger, M., Mihalache, M., Ohai, D. (2011) ″Researches regarding oxidation of nuclear grade materials in water at supercritical temperatures″, Techn. Meet. on Materials and Chemistry for Supercritical Water Cooled Reactors, Petten, The Neterlands.
[11] Fulger, M., Ohai, D., Mihalache, M., Fulger, S., Valeca, S.C. (2011) ″Analyses of oxide films grown on AISI 304L stainless steel and Incoloy 800HT exposed to supercritical water environment″, Journal of Nuclear Mater., Vol. 415, pp. 147–157.
[12] Tavares, S.S.M., Moura, V., da Costa, V.C., Ferreira, M.L.R., Pardal, J.M. (2009) ″Microstructural changes and corrosion resistance of AISI 310S steel exposed to 600–800 °C″, Material Charact., Vol. 60(6), pp. 573-578.